LLC LED Driver with Current-Sharing Capacitor Having Low Voltage Stress

Wen-Zhuang Jiang [1], Kuo-Ing Hwu [2,*] and Jenn-Jong Shieh [3]

[1] Chicony Power Technology Co., Ltd., Sanchong, New Taipei 24100, Taiwan; Vincent_Jiang@chiconypower.com.tw
[2] Department of Electrical Engineering, National Taipei University of Technology, 1, Sec. 3, Zhongxiao E. Rd., Taipei 10608, Taiwan
[3] Department of Electrical Engineering, Feng Chia University, No. 100, Wenhwa Road, Seatwen, Taichung 40724, Taiwan; jjshieh@fcu.edu.tw
[*] Correspondence: eaglehwu@ntut.edu.tw; Tel.: +886-2-27712171 (ext. 2159)

Abstract: In this paper, an LLC light-emitting diode (LLC LED) driver based on the current-sharing capacitor is presented. In the proposed LED driver, the LLC resonant converter is used to step down the high input voltage, to provide galvanic isolation, to offer a constant current for LEDs. Moreover, the current-sharing capacitor connected to the central-tapped point of the secondary-side winding is used to balance the currents in two LED strings. By doing so, the voltage stress on this capacitor is quite low. Above all, the equivalent forward voltages of the two LED strings are generally influenced by the temperature and the LED current, and this does not affect the current-sharing performance, as will be demonstrated by experiment on the difference in number of LEDs between the two LED strings. In addition, only the current in one LED string is sensed and controlled by negative feedback control, while the current in the other LED string is determined by the current-sharing capacitor. Moreover, this makes the current control so easy. Afterwards, the basic operating principles and analyses are given, particularly for how to derive the effective resistive load from the LED string. Eventually, some experimental results are provided to validate the effectiveness of the proposed LED driver.

Keywords: current-sharing capacitor; LED driver; LLC resonant converter

1. Introduction

As compared with the traditional lighting sources, like the incandescent lights, fluorescent lights, and halogen lights, etc., the high-brightness lighting-emitting diodes (LEDs) have become promising due to their long life, compact size, and eco-friendly characteristics [1]. The LED lights are widely used in the indoor lighting, outdoor lighting, and display backlighting. In these applications, multiple LEDs are connected to increase the luminous flux. The LEDs can be connected in series and parallel, depending on the output voltage and current of the LED driver. In general, multiple LEDs are connected in series to form an LED string, and then the LED strings are connected in parallel with each other. Since each LED has different voltage and current characteristics, the constant current control is required to equalize each LED string current. Therefore, LED current sharing technique is necessary. The LED current sharing can be classified into two methods. One is the active method [2–9], and the other is the passive method [10–15].

Generally, the active method uses semiconductor devices and integrated circuits to achieve LED current sharing. The active method has some disadvantages, such as complexity and high cost. The passive method, which features low cost and simplicity, is developed as another LED current sharing method. The passive method can be subdivided into inductive and capacitive methods. The inductive method usually uses the current-sharing transformers. For the current-sharing transformer method, the differential transformer

with a 1:1 turns ratio is used to balance the LED current. On the other hand, the capacitive method uses the capacitors to achieve LED current balance. The current sharing is achieved based on the capacitor ampere-second balance. In Figure 1, the literatures [14] and [15] display the low-power two-channel LED drivers using the capacitor to achieve LED current balance. They are suitable for low-input voltage and low-power applications. These two LED drivers are based on step-up converters. The output voltage of the two-channel LED driver is the sum of the voltages across two LED strings, and this is different from the parallel connection. Thus, these kinds of LED drivers are called pseudo multi-string LED drivers. However, if the resonance behavior is taken into account, then the soft switching of the switch and diode will happen, causing the overall efficiency can be upgraded. Consequently, the non-isolated boost resonant LED driver shown in [16] is presented. In this circuit, only the diode in the resonant path can have zero-current-switching (ZCS) turn-off. In addition, if the resonance behavior as well as galvanic isolation taking into consideration, then the isolated voltage-bucking resonant LED driver as displayed in [17] is proposed. In this circuit, only all the diodes on the secondary side have ZCS.
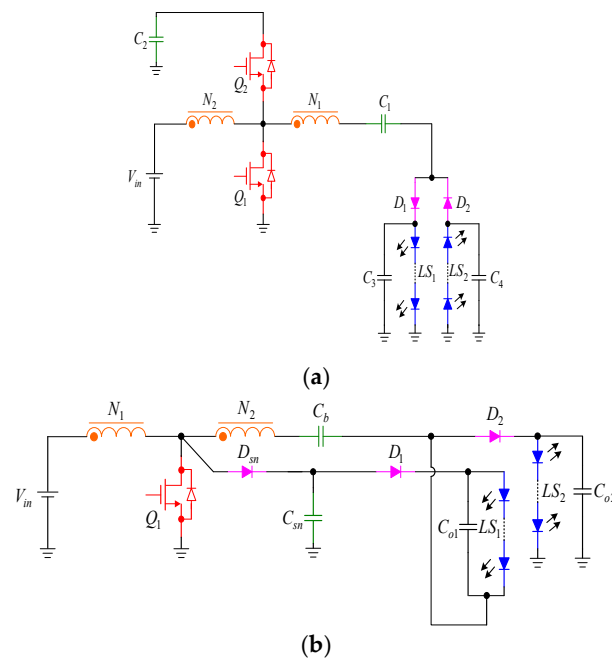

(a)

(b)

Figure 1. Prior work: (**a**) non-isolated two channel LED driver with automatic current balance and zero voltage switching [14]; (**b**) non-isolated single-switch two-channel LED driver with passive regenerative snubber [15].

Therefore, an isolated LED driver based on the LLC resonant converter is proposed herein. Both switches have zero-voltage-switching (ZVS) turn-on and both the diodes on the secondary side have ZCS turn-off except at light load. The proposed LED driver is based on the current-sharing capacitor with a quite low voltage stress. In this paper, the basic operating principles, steady-state analyses, and experimental results will be given in the following sections.

2. Basic Analysis of the Proposed LED Driver

Figure 2 shows the proposed two-channel LED driver. For analysis convenience, there are some assumptions to be made as follows.

(1)　The switches and components are ideal except for the metal-oxide-semiconductor field-effect transistor (MOSFET) switches and the transformer.

(2)　The values of all the capacitors are large enough. Thus, the voltages across them are regarded as constant.

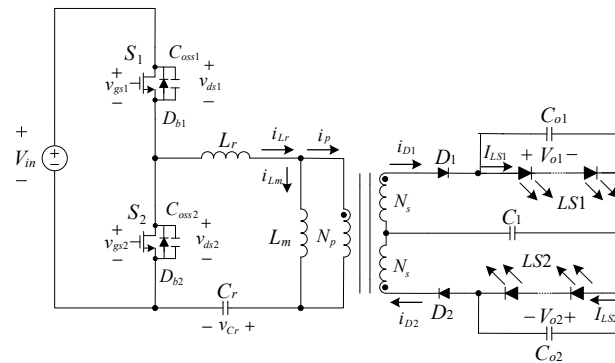(3) The two output voltages are identical, namely, $V_{o1} = V_{o2}$.

Figure 2. Proposed two-channel LLC resonant LED driver.

The following analyses contain the (a) operating principles; (b) LED modeling; (c) LED load characteristics; (d) voltage gain characteristics; and (e) extension of the proposed LED driver.

2.1. Operating Principles

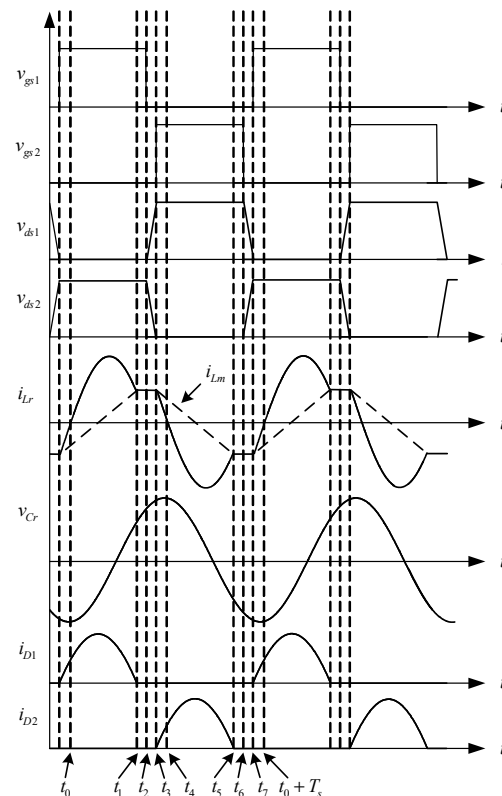There are 8 operating states in the proposed LED driver. Figure 3 shows the key waveforms over one switching period.

Figure 3. Key waveforms of the proposed LED driver over one switching period.

2.1.1. State 1 (t_0, t_1)

As shown in Figure 4a, S_1 is ON, but S_2 is OFF. Thus, L_r and C_r resonate with each other and i_{Lr} increases from zero. During this state, i_{Lr} is larger than i_{Lm}. Therefore, the current i_p is transferred from the primary side to the secondary side, thus making D_1

forward biased and hence providing energy to C_{o1} and $LS1$. As for $LS2$, it is powered by C_{o2}. At the same time, the voltage nV_{o1} is across L_m, thus causing i_{Lm} to be increased linearly. This state ends when i_{Lr} equals i_{Lm} at t_1.
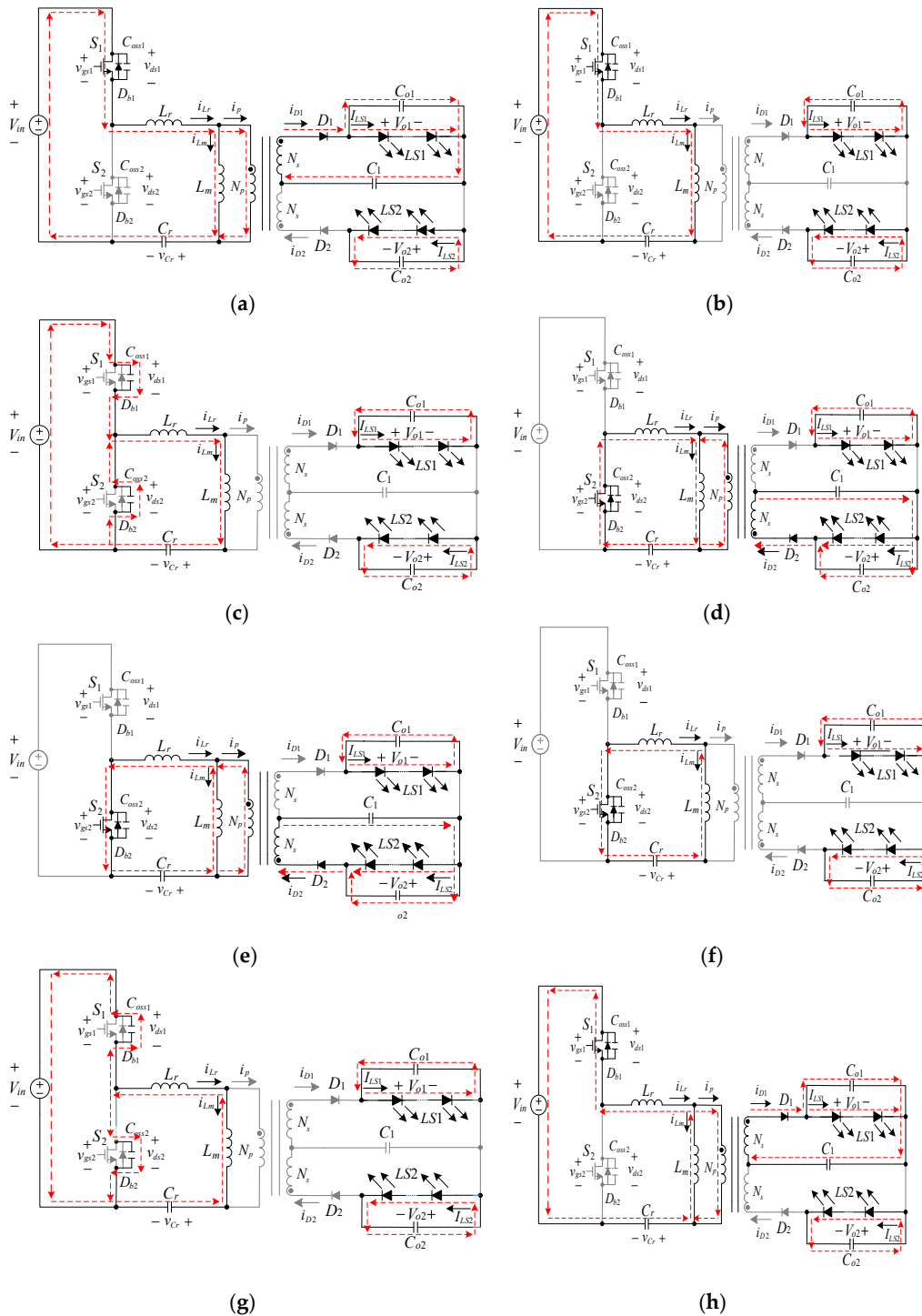

Figure 4. Operating circuits over one switching period: (**a**) state 1; (**b**) state 2; (**c**) state 3; (**d**) state 4; (**e**) state 5; (**f**) state 6; (**g**) state 7; (**h**) state 8.

2.1.2. State 2 (t_1, t_2)

As shown in Figure 4b, S_1 is still ON, but S_2 is still OFF. During this state, since i_{Lr} is equal to i_{Lm}, there is no current flowing through the secondary side, thereby causing the

energy required by $LS1$ and $LS2$ to be provided by C_{o1} and C_{o2}, respectively. At the same time, C_r, L_r, and L_m resonate together, thus causing i_{Lr} to be increased quite slowly. This state ends when S_1 turns off at t_2.

2.1.3. State 3 (t_2, t_3)

As shown in Figure 4c, S_1 is turned OFF and S_2 still keeps OFF. During this state, C_{oss1} is charged and C_{oss2} is discharged, thus causing the energy required by $LS1$ and $LS2$ to be still provided by C_{o1} and C_{o2}, respectively. This state ends when C_{oss1} is charged to V_{in}, and C_{oss2} is discharged to zero at t_3.

2.1.4. State 4 (t_3, t_4)

As shown in Figure 4d, S_1 keeps OFF, but S_2 is turned ON with zero voltage switching (ZVS) due to i_{Lr} flowing through D_{b2}. During this state, i_{Lr} is smaller than i_{Lm}. Therefore, the current $-i_p$ is reflected from the secondary side to the primary side, thereby making D_2 forward biased and hence providing energy to C_{o2} and $LS2$. As for $LS1$, it is powered by C_{o1}. At the same time, the voltage $-nV_{o2}$ is across L_m, thereby causing i_{Lm} to be decreased linearly. This state ends when i_{Lr} reaches zero at t_4.

2.1.5. State 5 (t_4, t_5)

As shown in Figure 4e, S_1 still keeps OFF, but S_2 keeps ON. During this state, i_{Lr} changes the direction. The voltage $-nV_{o2}$ is still across L_m. Thus, i_{Lm} is still decreased linearly. This state ends when i_{Lr} equals i_{Lm} at t_5.

2.1.6. State 6 (t_5, t_6)

As shown in Figure 4f, S_1 still keeps OFF, but S_2 still keeps ON. Since i_{Lr} is equal to i_{Lm}, there is no current flowing through the secondary side, thereby causing the energy required by $LS1$ and $LS2$ to be provided by C_{o1} and C_{o2}, respectively. At the same time, C_r, L_r and L_m resonate together, thus causing i_{Lr} to be decreased quite slowly. This state ends when S_2 turns off at t_6.

2.1.7. State 7 (t_6, t_7)

As shown in Figure 4g, S_1 still keeps OFF, and S_2 is turned OFF. During this state, C_{oss1} is charged and C_{oss2} is discharged, thus causing the energy required by $LS1$ and $LS2$ to be still provided by C_{o1} and C_{o2}, respectively. This state ends when C_{oss1} is discharged to zero, and C_{oss2} is charged to V_{in} at t_7.

2.1.8. State 8 (t_7, $t_0 + T_s$)

As shown in Figure 4h, S_2 keeps OFF, but S_1 is turned ON with ZVS due to i_{Lr} flowing through D_{b1}. During this state, $-i_{Lr}$ is smaller than $-i_{Lm}$. Therefore, the current i_p is transferred from the primary side to the secondary side, thus making D_1 forward biased and hence providing energy to C_{o1} and $LS1$. As for $LS2$ it is powered by C_{o2}. At the same time, the voltage nV_{o1} is across L_m, thus causing i_{Lm} to be increased linearly. This state ends when i_{Lr} reaches zero at $t = t_0 + T_s$.

2.2. LED Modeling

The LED string can be modeled as a piecewise linear model as shown in Figure 5. The equivalent LED string model contains one ideal diode D_{ideal}, one equivalent on-resistance R_{LED} and one equivalent forward voltage V_F, with all the three connected in series. Also, the LED string current is defined as I_{LED}. Hence, the LED string voltage V_{LED} can be expressed as
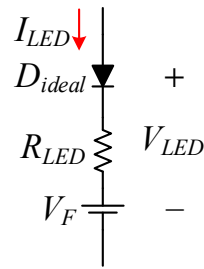
$$V_{LED} = V_F + I_{LED}R_{LED} \tag{1}$$

Figure 5. Approximately linear model of an LED string.

2.3. LED Load Characteristics

The AC equivalent load can be modeled by using the fundamental harmonic approximation (FHA). The AC equivalent circuit of the proposed LLC resonant LED driver is shown in Figure 6. The derivation is shown as follows.
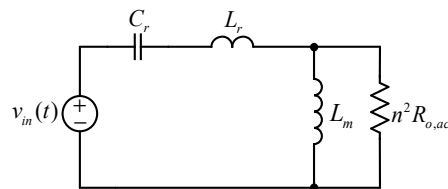

Figure 6. AC equivalent circuit of the proposed LED driver.

The current $i_{ac(fund)}$ is defined as a fundamental sinusoidal wave on the secondary side. That is,

$$i_{ac(fund)}(t) = I_p \sin(\omega_s t) \tag{2}$$

where I_p is the maximum value of $i_{ac(fund)}(t)$.

The expression of V_{LED} can be changed to

$$V_{LED} = V_F + R_{LED} I_{LED} = V_F + R_{LED} \langle i_{D1}(t) \rangle_{T_s} \tag{3}$$

where $\langle i_{D1}(t) \rangle_{T_s}$ is the average current of i_{D1} and equal to I_{LED}.

Therefore, $\langle i_{D1}(t) \rangle_{T_s}$ can be expressed to be

$$\langle i_{D1}(t) \rangle_{T_s} = \frac{1}{T_s} \int_0^{T_s/2} I_p |\sin(\omega_s t)| dt = \frac{1}{\pi} I_p \tag{4}$$

By substituting (4) into (3), V_{LED} can be rewritten to be

$$V_{LED} = V_F + R_{LED}(1/\pi) I_p \tag{5}$$

In addition, the voltage on the secondary side, $v_{ac}(t)$, can be expressed to be

$$v_{ac}(t) = \begin{cases} V_{o1}, & i_{D1}(t) > 0 \\ -V_{o2}, & i_{D2}(t) > 0 \end{cases} \tag{6}$$

Also, the voltage $v_{ac}(t)$ can be represented by a Fourier series as follows:

$$v_{ac}(t) = a_0 + \sum_{h=1}^{\infty} [a_h \cos(h\omega_s t) + b_h \sin(h\omega_s t)] \tag{7}$$

Since $v_{ac}(t)$ is an odd function waveform, a_n is zero. Thus,

$$v_{ac}(t) = \sum_{h=1,3,5,\ldots}^{\infty} \frac{4V_{o1}}{h\pi} \sin(h\omega_s t) \tag{8}$$

The fundamental waveform of $v_{ac}(t)$, called $v_{ac(fund)}(t)$, is

$$v_{ac(fund)}(t) = \left(\frac{4V_{o1}}{\pi}\right) \sin(\omega_s t) \tag{9}$$

Based (4) and $V_{o1} = V_{LED}$, the effective resistive load $R_{o,ac}$ can be signified by

$$R_{o,ac} = \frac{v_{ac(fund)}(t)}{i_{ac(fund)}(t)} = \frac{\left(\frac{4V_{o1}}{\pi}\right)\sin(\omega_s t)}{I_p \sin(\omega_s t)} = \frac{4V_{o1}}{\pi I_p} = \frac{4}{\pi^2}\left(\frac{V_{o1}}{I_{LED}}\right) = \frac{4}{\pi^2}\left(\frac{V_{LED}}{I_{LED}}\right) \tag{10}$$

2.4. Voltage Gain Characteristics

Figure 7 shows the two-port model of the FHA resonant circuit. The output load resistor R_{out} can be regarded as the equivalent static resistance of the LED string at a given forward current, that is, V_{LED} divided by I_{LED}. In addition, the voltage gain is

$$M(j2\pi f_s) = \frac{nV_{o,FHA}(j2\pi f_s)}{V_{in,FHA}(j2\pi f_s)} \tag{11}$$

where $V_{in,FHA}(j2\pi f_s)$ is the fundamental component of the input voltage in the phasor domain and $V_{o,FHA}(j2\pi f_s)$ is the fundamental component of the output voltage in the phasor domain.
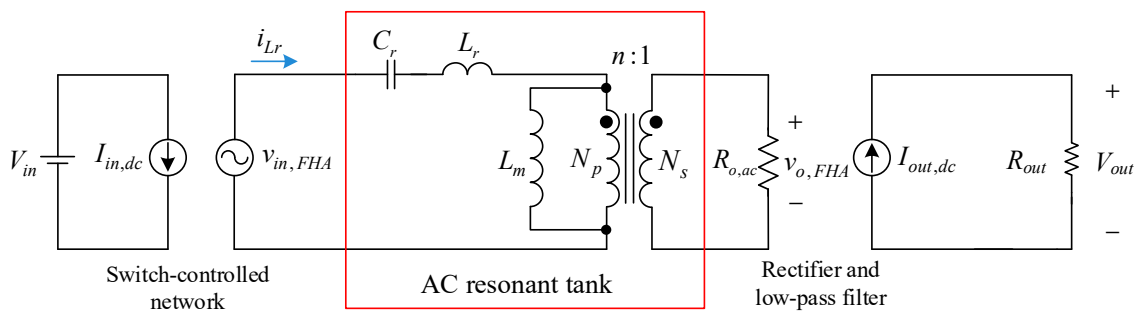
Figure 7. Two-port model of the FHA resonant circuit.

The input voltage waveform of the AC resonant tank is

$$v_{in}(t) = \frac{V_{in}}{2} + \sum_{h=1,3,5,\ldots}^{\infty} \frac{2V_{in}}{h\pi} \sin(h\omega_s t) \tag{12}$$

From (12), it can be seen that the fundamental component of the input voltage is

$$v_{in,FHA}(t) = \frac{2V_{in}}{\pi} \sin(\omega_s t) \tag{13}$$

As derived in (9), the output voltage fundamental component is

$$v_{o,FHA}(t) = v_{ac(fund)}(t) = \left(\frac{4V_{o1}}{\pi}\right) \sin(\omega_s t) \tag{14}$$

Based on (11), (13), and (14), the DC-DC input-to-output voltage conversion ratio can be derived as follows:

$$|M(j2\pi f_s)| = \frac{n|V_{o,FHA}(j2\pi f_s)|}{|V_{i,FHA}(j2\pi f_s)|} = \frac{n\left(\frac{4V_{o1}}{\pi}\right)}{\frac{2V_{in}}{\pi}} \tag{15}$$

From (15), the DC-DC input-to-output voltage conversion ratio is

$$\frac{V_{o1}}{V_{in}} = \frac{1}{2n}|M(j2\pi f_s)| \tag{16}$$

In Figure 6, by transferring the time domain to the s domain and let $s = j2\pi f_s$, the magnitude of the voltage gain $M(j2\pi f_s)$, called M, can be derived as follows:

$$M = |M(j2\pi f_s)| = \frac{K \times \left(\frac{f_s}{f_r}\right)^2}{\sqrt{\left[(K+1) \times \left(\frac{f_s}{f_r}\right)^2 - 1\right]^2 + \left\{[(\frac{f_s}{f_r})^3 - 1] \times \frac{f_s}{f_r} \times Q \times K\right\}^2}} \tag{17}$$

where $K = \frac{L_m}{L_r}$, $f_r = \frac{1}{2\pi\sqrt{L_r C_r}}$, $Q = \frac{Z_o}{n^2 R_{o,ac}}$, and $Z_o = \sqrt{\frac{L_r}{C_r}}$.

From (17), it can be seen that Q and K will affect the voltage gain.

The output resistance in Figure 7 is replaced with the LED equivalent model as shown in Figure 8. Based on (1),

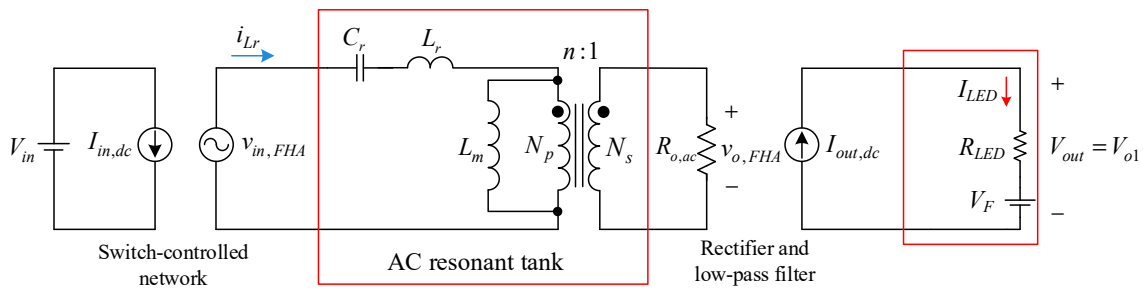$$I_{LED} = \frac{V_{LED}(= V_{o1}) - V_F}{R_{LED}} \tag{18}$$

Figure 8. Two-port model of the FHA resonant circuit with one LED string at the output terminals.

Based on (16), Equation (19) can be rewritten as

$$I_{LED} = \frac{|M(j2\pi f_s)| \cdot \frac{V_{in}}{2n} - V_F}{R_{LED}} \tag{19}$$

From (19), it can be seen that the LED current can be regulated by changing the switching frequency f_s, and this means that the gain adjustment is made by frequency modulation. As seen in Figure 9, by giving an LED current command $I_{LED\_command}$, the frequency modulator will change the switching frequency f_s, and $v_{o,FHA}$ will be varied to a corresponding value according to the designed voltage gain M.
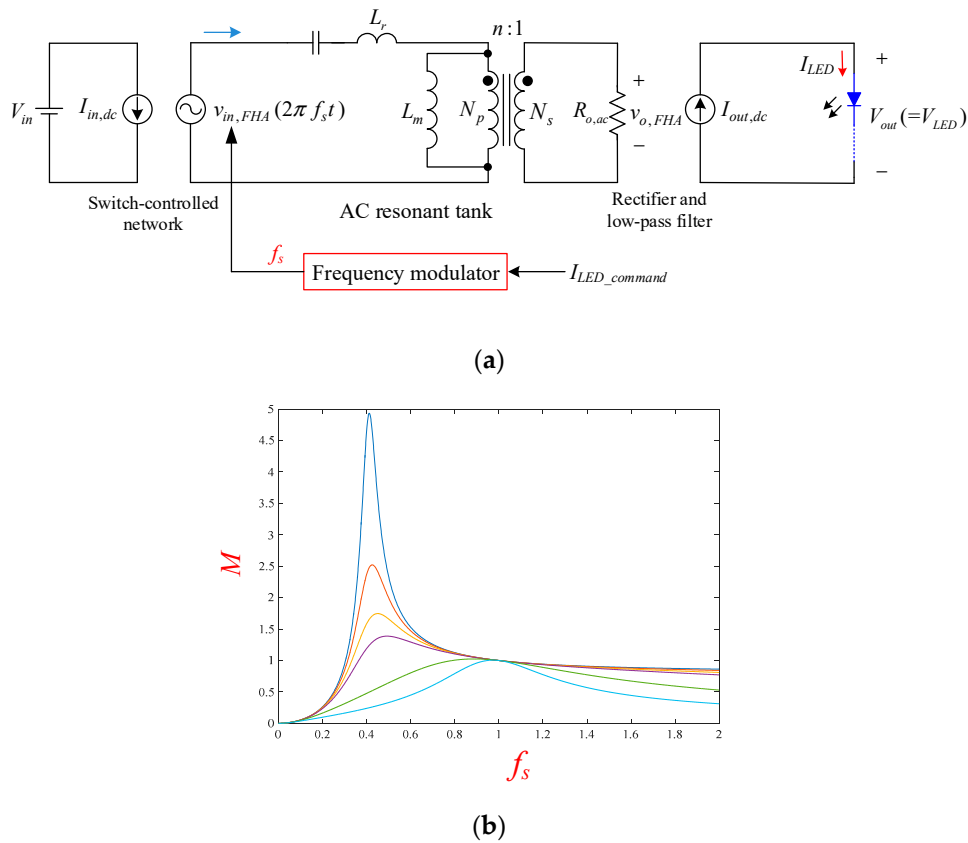
(a)

(b)

Figure 9. Two-port model of the FHA resonant circuit with: (**a**) frequency modulator; (**b**) voltage gain M versus switching frequency f_s.

2.5. System Control

Figure 10 shows the control strategy of the proposed LED driver. From Figure 10a, it can be seen that one of the LED strings is sensed and the current signal is transformed to the voltage signal and then sent to UCD3138, which contains an error ADC, a filter, and a digital PWM as shown in Figure 10b. The sensed current signal will be sent to the error ADC and compared with the prescribed reference value. After this, the error signal will be sent to the filter, called the PID controller. Eventually, the calculated duty cycle and frequency will control the MOSFETs to regulate the LED string currents.
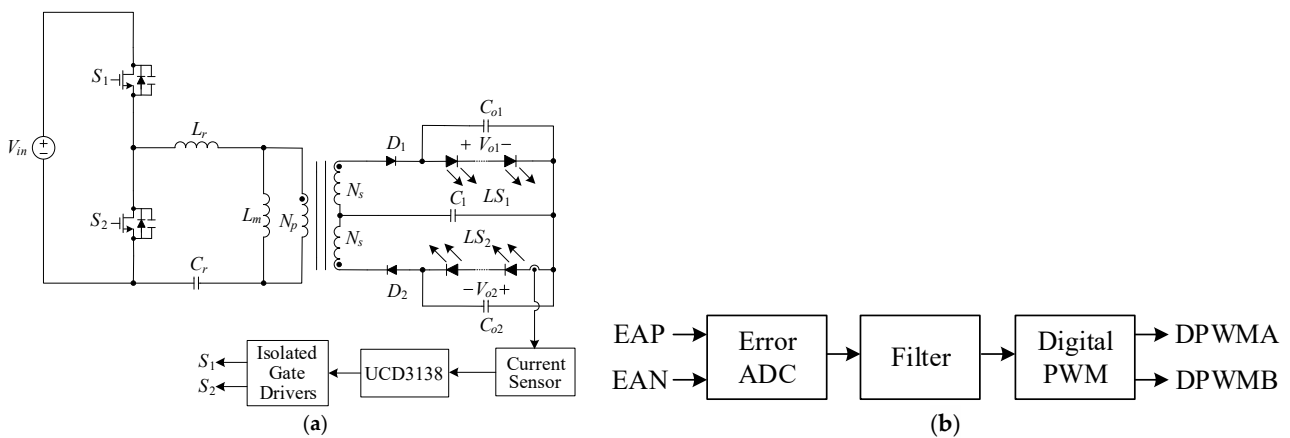

(a)

(b)

Figure 10. System control: (**a**) block diagram; (**b**) UCD3138 control kernel.

2.6. Effect of Variations in Equivalent forward Voltage on Current Sharing

As shown in Figure 10a, since the voltages across the two central-tapped windings are the same, this means that

$$V_{D1} + V_{o1} - V_{C1} = V_{D2} + V_{o2} + V_{C1} \tag{20}$$

Assuming that the diodes D_1 and D_2 are two-in-one, V_{D1} can be regarded as almost equal to V_{D2}. Therefore, (20) can be simplified to (21):

$$V_{C1} = 0.5 \times (V_{o1} - V_{o2}) \tag{21}$$

Based on (21), if the two LED strings are identical, then V_{C1} is zero; otherwise, V_{C1} is not zero. This means that the difference in equivalent forward voltage between the two LED strings can be absorbed by the current-sharing capacitor C_1.

2.7. Circuit Extension

Figure 11 shows the four-channel LED driver, which can be derived from the proposed two-channel LED driver. However, in practice, the effective resistive load $R_{o,ac}$ will be changed. Consequently, the design of the associated parameters will be repeated if necessary.
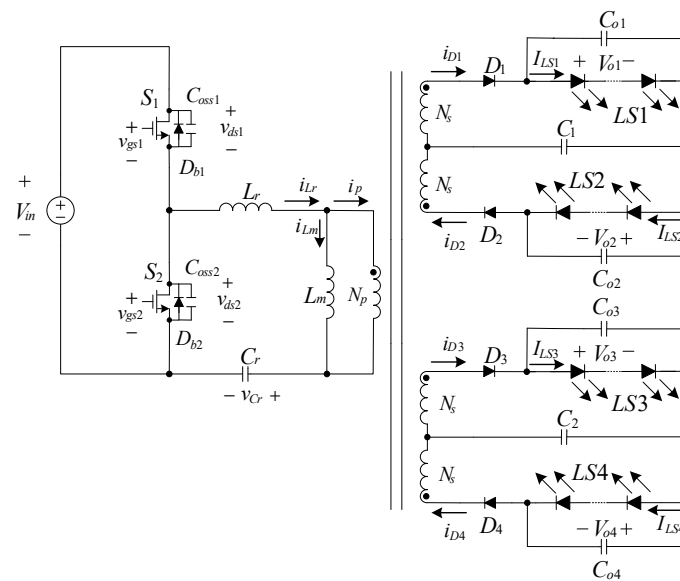

Figure 11. Four-channel LED driver derived from the proposed LED driver.

3. Design Considerations

To verify the effectiveness of the proposed LED driver, a prototype is built up and tested. Table 1 shows the system specifications of the proposed converter, whereas Table 2 shows the component specifications used in the proposed converter. Moreover, the design procedures of (a) LED selection; (b) transformer turns ratio (n); (c) maximum voltage conversion ratio (M_{max}) and minimum voltage conversion ratio (M_{min}); (d) effective resistive load reflected to the primary side of the transformer ($n^2 R_{o,ac}$); (e) ratio of magnetizing inductance to resonant inductance ratio (K) and quality factor (Q); and (f) resonant capacitance (C_r), resonant inductance (L_r), and magnetizing inductance (L_m).

Table 1. System specifications of the proposed LED driver.

System Parameters	Specifications
Normal input voltage (V_{in_nor})	400 V
Maximum input voltage (V_{in_max})	410 V
Minmimum input voltage (V_{in_min})	390 V
Nominal LED channel voltage (V_{o1}, V_{o2})	3.45 V $\times$ 12 = 41.4 V
Nominal LED channel current (i_{o1}, i_{o2})	350 mA
Nominal LED power value (P_{LED})	30 W
Resonant frequency (f_r)	100 kHz
Ratio of magnetizing inductance to resonant inductance (K)	5
Quality factor (Q)	0.48

Table 2. Components used in the proposed LED driver.

Components	Specifications
MOSFET switches (Q_1, Q_2)	SPA20N60C3
Diodes (D_1, D_2)	80 CPQ 150 PbF
Resonant capacitor (C_r)	3.3 nF
Transformer (T_1)	Core: PQ35/35 $n = N_p/N_s = 60/12$, L_m = 230.074 μH, L_{lk} = 9.88 μH,
Resonant inductor (L_r)	Core: PQ20/20 L_r = 965.8 μH
Current-sharing capacitor (C_1)	10 μF
Output capacitors (C_{o1}, C_{o2})	10 μF

3.1. Selection of LED String

The high-power LEDs, used as load for the proposed LED driver, are made by Everlight Electronics Ltd. The corresponding product name is EHP-AX08EL/GT01H-P01/5670/Y/K42. From the associated datasheet, it can be seen that the forward voltage is about 3.45 V if the constant current flowing through the LED is 350 mA. In the proposed two-channel LED driver, 12 pieces of LEDs are connected in series for each string. Also, the LED string can be constructed by as an approximately linear model as shown in Figure 5. The equivalent forward voltage V_F is about 41.4 V (= 2.73·12), and the equivalent on-resistance R_{LED} is about 24.68 Ω (= 2.057·12).

3.2. Determination of Transformer Turns Ratio

The turns ratio of the transformer can be figured out under normal input voltage and unity voltage gain, namely, M_{nor} = 1:

$$n = M_{nor} \times \frac{1}{2} \times \frac{V_{in\_nor}}{V_{o\_rated}} = 1 \times \frac{1}{2} \times \frac{400}{41.4} \approx 4.83 \tag{22}$$

Based on the above calculation, the turns ratio n is selected to be 5. Via recalculation, the new voltage gain is 1.04.

3.3. Maximum and Minimum Voltage Gains

The maximum voltage gain and the minimum voltage gain are calculated as follows:

$$M_{max} = 2 \times n \times \frac{V_{o\_rated}}{V_{in\_min}} = 2 \times 5 \times \frac{41.4}{390} \approx 1.06 \tag{23}$$

$$M_{min} = 2 \times n \times \frac{V_{o\_rated}}{V_{in\_max}} = 2 \times 5 \times \frac{41.4}{410} \approx 1.01 \tag{24}$$

To prevent the operating point from going into the capacitive region, the maximum voltage gain should have a margin. The corresponding margin is 0.15 times M_{max}. Therefore, the value of M_{max} is changed to

$$M_{max} = 1.06 \times 1.15 \approx 1.22 \tag{25}$$

3.4. Effective Resistive Load on the Primary Side

Based on (10), the effective resistive load on the primary side, R_{ac}, is calculated as follows:

$$R_{ac} = n^2 R_{o,ac} = n^2 \frac{4}{\pi^2} \frac{V_{o\_rated}}{I_{LED}} = 5^2 \times \frac{4}{\pi^2} \times \frac{41.4}{0.35} \approx 1198.49 \ \Omega \tag{26}$$

3.5. Selection of K and Q and Determination of Switching Frequency Range

In the proposed LED driver, the value of K is selected to be 5. From Figure 12, it can be seen that the values of M change with different values of Q. In this paper, Q is selected to be 0.48. The minimum switching frequency f_{s_min} and the maximum switching frequency f_{s_max} are shown below:

$$f_{s\_min} = \frac{f_r}{\sqrt{1 + K(1 - \frac{1}{M_{max}^2})}} = \frac{100 \times 10^3}{\sqrt{1 + 5 \times (1 - \frac{1}{1.22^2})}} = 61.5 \ \text{kHz} \tag{27}$$

$$f_{s\_max} = \frac{f_r}{\sqrt{1 + K(1 - \frac{1}{M_{min}})}} = \frac{100 \times 10^3}{\sqrt{1 + 5 \times (1 - \frac{1}{1.01})}} = 97.7 \ \text{kHz} \tag{28}$$
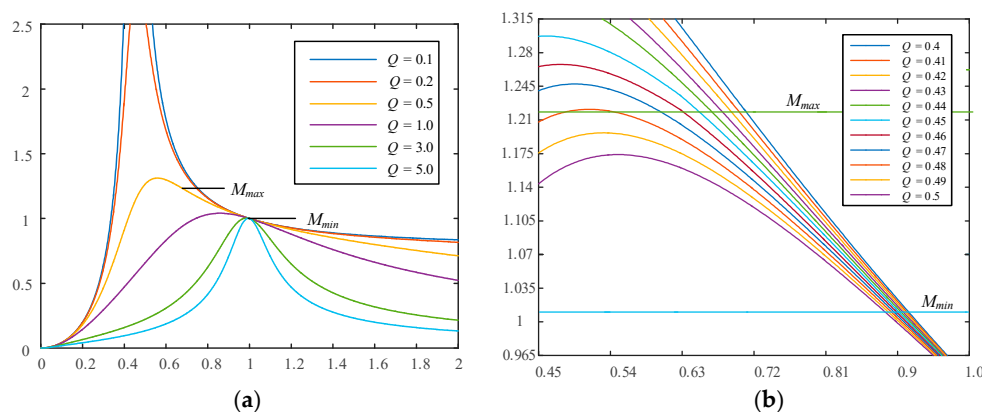

Figure 12. Voltage gain with K = 5: (**a**) original; (**b**) zoom-in.

3.6. Resonant Capacitance, Resonant Inductance and Magnetizing Inductance

Based on the effective resistive load calculated in (26), the selected resonant frequency f_r = 100 kHz, and the selected quality factor Q = 0.48, the resonant capacitance C_r can be worked out from (29). Moreover, based on (29), the resonant inductance L_r can be figured out from (30). Finally, based on the selected K = 5, the magnetizing inductance can be found from (31):

$$Q = \sqrt{\frac{L_r}{C_r}} \times \frac{1}{R_{ac}} = \frac{1}{2\pi \times f_r \times R_{ac} \times C_r}$$
$$\Rightarrow C_r = \frac{1}{2\pi \times Q \times f_r \times R_{ac}} \tag{29}$$
$$\Rightarrow C_r = \frac{1}{2\pi \times 0.48 \times 100 \times 10^3 \times 1198.49} = 2.767 \ \text{nF}$$

$$f_r = \frac{1}{2\pi \sqrt{L_r \times C_r}}$$
$$\Rightarrow L_r = \frac{1}{(2\pi \times f_r)^2 \times C_r} \tag{30}$$
$$\Rightarrow L_r = \frac{1}{(2\pi \times 100 \times 10^3)^2 \times 2.767 \times 10^{-9}} = 915.6 \ \mu\text{H}$$

$$L_m = K \times L_r = 5 \times 915.6\mu = 4578 \ \mu\text{H} \tag{31}$$

4. Experimental Results

Figures 13–18 show the measured waveforms at rated loads. Figure 13 shows the gate driving signals for the switches Q_1 and Q_2, and the voltage stresses v_{ds1} and v_{ds2}. From this figure, it can be seen that the voltage stresses on Q_1 and Q_2 are around 400 V.
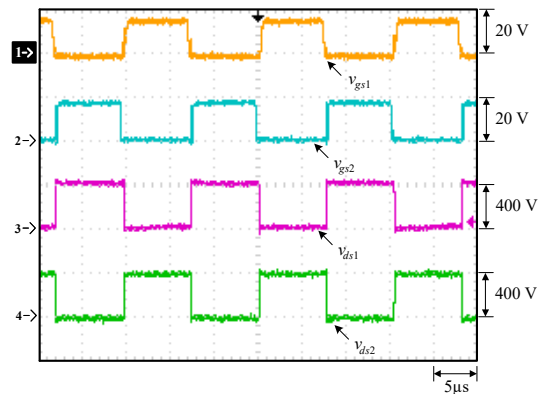

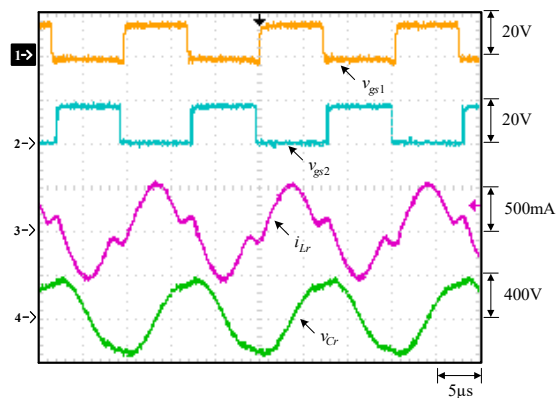**Figure 13.** Waveforms at rated load: (1) v_{gs1}; (2) v_{gs2}; (3) v_{ds1}; (4) v_{ds2}.

Figure 14. Waveforms at rated load: (1) v_{gs1}; (2) v_{gs}; (3) i_{Lr}; (4) v_{Cr}.
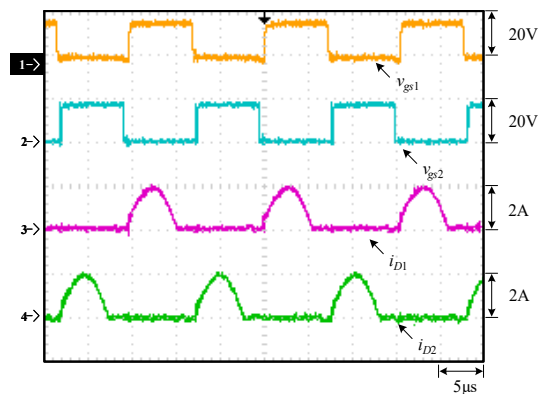
Figure 15. Waveforms at rated load: (1) v_{gs1}; (2) v_{gs2}; (3) i_{D1}; (4) i_{D2}.
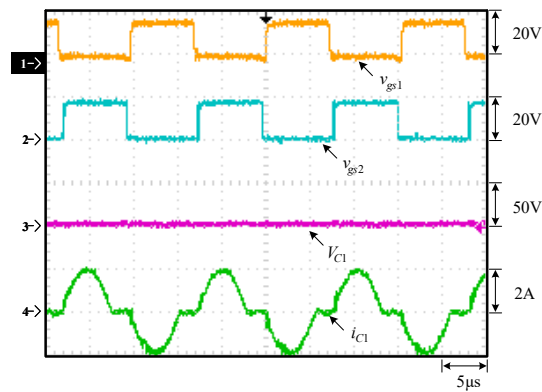
Figure 16. Waveforms at rated load: (1) v_{gs1}; (2) v_{gs2}; (3) V_{C1}; (4) i_{C1}.
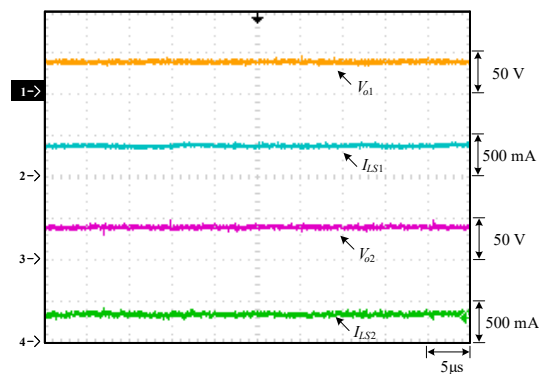

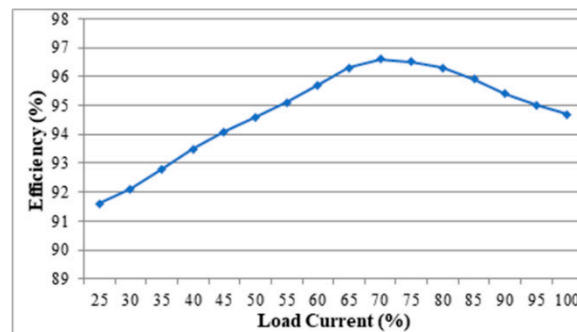**Figure 17.** Waveforms at rated load: (1) V_{o1}; (2) I_{LS1};(3) V_{o2}; (4) I_{LS2}.

Figure 18. Measured efficiency.

Figure 14 displays the resonant inductor current i_{Lr}, and the resonant capacitor voltage v_{Cr}. From this figure, it can be seen that the switching frequency f_s is smaller than the resonant frequency f_r. Also, when the resonant inductance current equals the magnetizing inductance current, there is no current transferring to the secondary side. During this period, C_r, L_r and L_m resonate together, resulting in a slow increase of the resonant current.

Figure 15 shows the diode currents. From this figure, it can be seen that the diode currents reach zero before the MOSFET switches are turned on, and this means that the diodes are turned off with zero-current switching (ZCS).

Figure 16 shows the voltages on the two LED strings, named V_{o1} and V_{o2}, and the currents in the two LED strings, named I_{LS1} and I_{LS2}. From this figure, it can be seen that V_{o1} and V_{o2} are both about 41 V, and I_{SL1} and I_{SL2} are regulated to be 350 mA.

Figure 17 displays the voltage across C_1, named V_{C1}, and current flowing through C_1, named i_{C1}. From this figure, it can be seen that V_{C1} is zero due to V_{o1} almost equal to V_{o2}.

Figure 18 displays the efficiency. From this figure, it can be seen that the rated-load efficiency is around 94.8%, and the highest efficiency is around 96.6%.

Furthermore, in order to verify the current-sharing performance of variations in forward voltage due to the temperature and the LED current, the number of LEDs for LS_1 is 12 LEDs and the number of LEDs for LS_2 is 9 LEDs. From Figure 19, it can be seen that two currents in $LS1$ and $LS2$ are almost the same, about 350 mA, but the difference in voltage between $LS1$ and $LS2$ is 10 V (= $V_{o1} - V_{o2}$ = 40 V − 30 V = 10 V). From this result, it is obvious that if the forward voltage is varied due to the temperature and the LED current, the current sharing is still performed well.
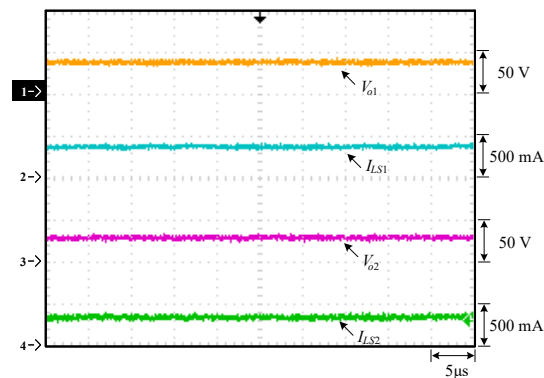

Figure 19. Measured waveforms under a difference in LED count between the two LED strings: (1) V_{o1}; (2) I_{LS1}; (3) V_{o2}; (4) I_{LS2}.

In Figure 20, it can be seen that the voltage across C_1 is not zero, equal to about 5 V, which can be obtained based on (21).
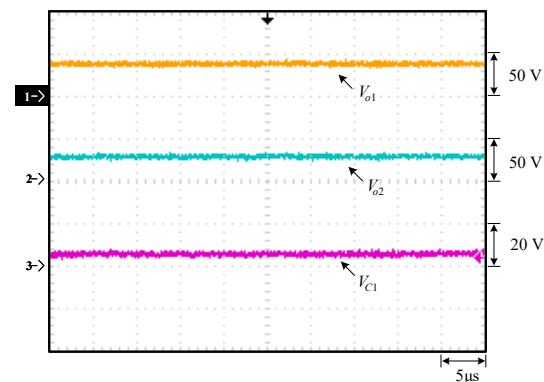

Figure 20. Measured waveforms under a difference in LED count between the two LED strings: (1) V_{o1}; (2) V_{o2}; (3) V_{C1}.

In addition, as shown in Figure 18, the current consumed by the system can be calculated based on output power divided by efficiency and input voltage. Accordingly, the current consumed at 25% load current with 91.6% efficiency is 0.02047 A, the current consumed at 70% load current with 96.6% efficiency is 0.05435 A, and the current consumed at 100% load current with 94.8% efficiency is 0.07911 A.

5. Comparison of Waveforms and Efficiencies

In the following, Figure 17 is compared with Figures 21 and 22, whereas Figure 18 is compared with Figures 23 and 24. From Figures 17, 21 and 22, it can be seen that the currents in two LED strings for each figure are almost the same. Since the input voltages in [14] and [15] are of 3.3 V ± 10%, the number of efficiency curves for each of these two literatures

is three. The highest efficiency among Figures 18, 23 and 24 is 96.6% from Figure 18, whereas the lowest efficiency among them is 86.5% from Figure 24.
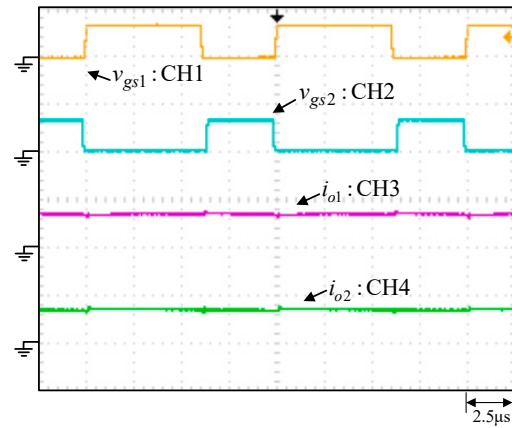

Figure 21. Waveforms at input voltage of 3.3 V [14]: (1) v_{gs1} (20 V/div); (2) v_{gs2} (20 V/div); (3) i_{o1} (500 mA/div); (4) i_{o2} (500 mA/div).
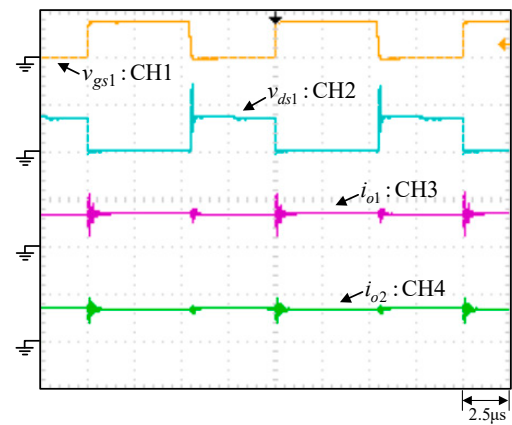

Figure 22. Waveforms at input voltage of 3.3 V [15]: (1) v_{gs1} (20 V/div); (2) v_{ds1} (10 V/div); (3) i_{o1} (500 mA/div); (4) i_{o2} (500 mA/div).
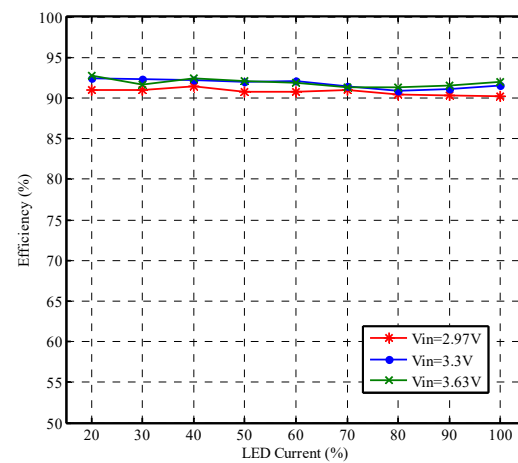

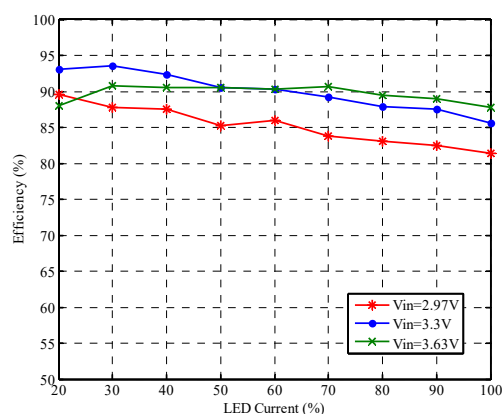**Figure 23.** Measured efficiency versus LED current [14].

Figure 24. Measured efficiency versus LED current [15].

6. Conclusions

An isolated LED driver based on the LLC resonant converter is presented herein. In the proposed LED driver, the current-sharing capacitor is used to balance the LED currents. Therefore, the active current sharing circuits are not required. From the experimental results, it can be seen that the currents in the two LED strings are identical without considering the difference in equivalent forward voltage between the two LED strings. Furthermore, the number of the LED channels can be increased. A detailed design of the proposed LED driver is shown in this paper, particularly for how to obtain the effective resistive load from the LED string. As for current control, only the current in one LED string is sensed and controlled by negative feedback control, and the current in the other LED string is determined by the current-sharing capacitor. By doing so, this makes the current control quite easy. Moreover, the measured efficiency shows that the efficiency at rated load is around 94.8%, and the efficiency can be up to 96.6%.

Institutional Review Board Statement: Not applicable.

Informed Consent Statement: Not applicable.

Data Availability Statement: No new data were created or analyzed in this study. Data sharing is not applicable to this article.

Conflicts of Interest: The authors declare no conflict of interest.

References

1. Shur, M.S.; Zukauskas, A.R. Solid-State Lighting: Toward Superior Illumination. *Proc. IEEE* **2005**, *93*, 1691–1703. [CrossRef]
2. Ke, B.; Lin, W. A Novel Current Sharing Method without the Signal Line for Multi-Output LED Driver. In Proceedings of the 11th China International Forum on Solid State Lighting (SSLCHINA), Guangzhou, China, 6–8 November 2014; pp. 19–22.
3. Chiu, H.-J.; Cheng, S.-J. LED Backlight Driving System for Large-Scale LCD Panels. *IEEE Trans. Ind. Electron.* **2007**, *54*, 2751–2760. [CrossRef]
4. Hwu, K.-I.; Yau, Y.T. Applying One-Comparator Counter-based Sampling to Current Sharing Control of Multi-Channel Led Strings. In Proceedings of the 25th Annual IEEE Applied Power Electronics Conference and Exposition (APEC), Palm Springs, CA, USA, 21–25 February 2010; pp. 737–742.

5. Chiu, H.-J.; Lo, Y.-K.; Chen, J.-T.; Cheng, S.-J.; Lin, C.-Y.; Mou, S.-C. A High-Efficiency Dimmable LED Driver for Low-Power Lighting Applications. *IEEE Trans. Ind. Electron.* **2010**, *57*, 735–743. [CrossRef]
6. Hu, Y.; Jovanovic, M.M. LED Driver with Self-Adaptive Drive Voltage. *IEEE Trans. Power Electron.* **2008**, *23*, 3116–3125. [CrossRef]
7. Li, S.N.; Zhong, W.X.; Chen, W.; Hui, S.Y.R. Novel Self-Configurable Current-Mirror Techniques for Reducing Current Imbalance in Parallel Light-Emitting Diode (LED) Strings. *IEEE Trans. Power Electron.* **2012**, *27*, 2153–2162. [CrossRef]
8. Hwu, K.-I.; Lai, C.-Y.; Tu, W.-C. Light-emitting diode driver with low-frequency ripple suppressed and dimming efficiency improved. *IET Power Electron.* **2014**, *7*, 105–113. [CrossRef]
9. Yu, W.; Lai, J.-S.; Ma, H.; Zheng, C. High-Efficiency DC–DC Converter with Twin Bus for Dimmable LED Lighting. *IEEE Trans. Power Electron.* **2011**, *26*, 2095–2100. [CrossRef]
10. Hwu, K.I.; Chou, S.-C. A Simple Current-Balancing Converter for LED Lighting. In Proceedings of the 24th Annual IEEE Applied Power Electronics Conference and Exposition, Washington, DC, USA, 15–19 February 2009; pp. 587–590.
11. Hwu, K.-I.; Tu, W.C.; Hong, M.-J. A Led Current Balancing Driver with Magnetizing Inductance Energy Recycling Considered. In Proceedings of the 27th Annual IEEE Applied Power Electronics Conference and Exposition (APEC), Orlando, FL, USA, 5–9 February 2012; pp. 975–979.
12. Hwu, K.-I; Tu, W.C.; Hong, M.J. A Dimmable LED Driver Based on Current Balancing Transformer with Magnetizing Energy Recycling Considered. *J. Disp. Technol.* **2014**, *10*, 388–395. [CrossRef]
13. Lin, Y.-L.; Chiu, H.-J.; Lo, Y.-K.; Leng, C.-M. Light-Emitting Diode Driver with a Combined Energy Transfer Inductor for Current Balancing Control. *IET Power Electron.* **2015**, *8*, 1834–1843. [CrossRef]
14. Hwu, K.I.; Jiang, W.Z. Nonisolated Two-Channel LED Driver with Automatic Current Balance and Zero-Voltage Switching. *IEEE Trans. Power Electron.* **2016**, *31*, 8359–8370. [CrossRef]
15. Hwu, K.-I.; Jiang, W.Z. Single-Switch Coupled-Inductor-Based Two-Channel LED Driver with a Passive Regenerative Snubber. *IEEE Trans. Power Electron.* **2017**, *32*, 4482–4490. [CrossRef]
16. Liu, X.; Zhou, Q.; Xu, J.; Lei, Y.; Wang, P.; Zhu, Y. High-Efficiency Resonant LED Backlight Driver with Passive Current Balancing and Dimming. *IEEE Trans. Ind. Electron.* **2018**, *65*, 5476–5486. [CrossRef]
17. Liu, X.; Yang, Q.; Zhou, Q.; Xu, J.; Zhou, G. Single-Stage Single-Switch Four-Output Resonant LED Driver with High Power Factor and Passive Current Balancing. *IEEE Trans. Power Electron.* **2017**, *32*, 4566–4576. [CrossRef]